Journal of Alloys and Compounds 980 (2024) 173565

Contents lists available at ScienceDirect

Journal of Alloys and Compounds

journal homepage: www.elsevier.com/locate/jalcom

Engineering yttrium oxide antioxidant nanoagents

Albenc Nexha, Francesc Díaz, Magdalena Aguiló, Maria Cinta Pujol, Joan Josep Carvajal *

Universitat Rovira i Virgili, Departament Química Física i Inorgànica, Física i Cristal·lografia de, Materials i Nanomaterials (FiCMA-FiCNA)-EMaS, Campus Sescelades, E-43007 Tarragona, Spain

ARTICLE INFO

Keywords:
Wet chemical syntheses
Yttrium oxide nanocrystals
Hydroxyl radical scavenging
Fenton assay
Ex-vivo antioxidant

ABSTRACT

Yttrium oxide nanocrystals with different sizes and shapes, are synthesized via thermal decomposition and digestive ripening-assisted methodologies. From the thermal decomposition methodology, nanotriangles and nanohearts, with lateral sizes around 25 nm and 35 nm, respectively, are produced. From the digestive ripening methodology, self-assembled nanodiscs with diameters up to 22 nm and thicknesses down to their unit cell, were synthesized. After rendering these nanocrystals water soluble, their ability to scavenge harmful hydroxyl radicals, is tested by applying a Fenton assay. Several factors affected the scavenging properties of these nanocrystals, including their concentration, morphology, and dopants. The antioxidant properties were enhanced for concentrations up to 1 mg mL^{-1}. Higher concentrations induced oxidant properties. Nanotriangles were able to scavenge more hydroxyl radicals compared to the other two shapes due to their higher surface area. Adding dopants into the nanotriangles, such as Er^{3+} and Yb^{3+}, enhanced further the scavenging properties. The scavenging properties of yttrium oxide nanocrystals were comparable to state of the art cerium oxide particles, which opened the avenue to explore further the capabilities of these nanocrystals as *ex-vivo* scavengers. In this vein, an *ex-vivo* experiment was designed as a proof of concept to prove the hydroxyl radical scavenging properties of yttrium oxide nanoparticles in biological media.

1. Introduction

Reactive oxygen species (ROS) are unstable chemicals, which react quickly with other molecules within a medium [1–6]. Among them, hydroxyl radicals (•OH) are the strongest oxidants [1,2]. When the concentration of these radicals exceeds a certain level in biological media, a series of irreversible damages are initiated, including oxidative stress, mutations and cell death [7–10]. The generation of these radicals is triggered by the interaction of biomolecules containing metals such as Cu^{+} or Fe^{2+}, with hydrogen peroxide (H_2O_2) [1,2,10,11]. For example, during chronic alcoholic consumption, the levels of Cu^{+} or Fe^{2+} in the cells are increased, which promotes the generation of •OH species [12,13]. Thus, quantification and regulation of the levels of •OH under physiological conditions, is a crucial, yet challenging task.

Strategies to control and prevent the generation of •OH are addressed by the development of antioxidant agents. These agents are applied in multiple fields ranging from therapies to food and industrial technologies. For example, antioxidants are applied to the treatment of hypertension [14], or brain injuries [15]. In food technology, they are key components in preserving the quality of fats, oils and lipids by suppressing oxidation reactions of their unsaturated components [16]. They are also applied as stabilizers in fuels to prevent oxidation, and in gasolines to avoid polymerization, a process that leads to the formation of engine-fouling residues [17]. Therefore, the development of new materials as potential antioxidant agents is highly demanded in multiple areas.

The main class of antioxidant compounds that have been extensively investigated are defective metal oxide nanoparticles due to their rich active sites and excellent stability [2,18]. Typical types of metal oxide nanoparticles applied as antioxidants involve transition [19–22], and lanthanide metals [13,23–28]. Among these, lanthanide based oxides have triggered the development of antioxidants, with the principal material being cerium oxide, CeO_2 (also known as ceria). Ceria particles have been established as antioxidant agents, due to their ability to switch between Ce^{4+} and Ce^{3+} oxidation states on their surfaces [13,25,29]. In parallel, their good biocompatibility properties have boosted their applicability, for example towards prevention of retinal degradation induced by intracellular peroxide molecules [30], protection from radiation-induced pneumonitis [31], treatment of hepatocellular carcinoma [32], and generation of cardio protective effects [33]. The

* Corresponding author.
E-mail address: joanjosep.carvajal@urv.cat (J.J. Carvajal).

https://doi.org/10.1016/j.jallcom.2024.173565
Received 2 November 2023; Received in revised form 13 December 2023; Accepted 15 January 2024
Available online 17 January 2024

antioxidant properties of ceria particles are closely related to their size and shape, the coating and charge of the surface, doping, oxygen vacancies, and other external factors including the pH of the medium or the nature of the buffer [34].

Herein, we analyze the antioxidant properties of yttrium oxide (Y_2O_3, also known as yttria) nanocrystals as a potential •OH scavenger. Schubert *et al.*[35] not only highlighted the ability of yttria to protect nerve cells from oxidative stress, but concluded that these particles have superior antioxidant properties compared to ceria. Additional studies suggest that yttria particles prevent photoreceptors death in a light-damage model of retinal degeneration [26], and reduce the severity of acute pancreatitis [36]. These nanoparticles were also investigated as prophylactic and therapeutic antioxidant agents on heat stressed models [37]. Yttria can also act as host material for doping [38–44], due to its broad transparency range (0.2–8 μm), with a wide band gap of 5.6 eV, and low phonon energy [45,46]. In addition, yttria nanoparticles are benign in in-vitro [35], or in-vivo systems [47], which renders them as potential candidate for biomedical applications. Yttria, as ceria, displays some degree of nonstoichiometry [48,49]. The nonstoichiometric characteristics of yttria are exhibited under normal conditions of temperature and pressure [50,51], and can be visualized through the absorption of water and carbon dioxide from the atmosphere [52]. Up to date, it is believed that are these nonstoichiometric characteristics that renders yttria its antioxidant properties [35].

Concerning antioxidant experiments based on optical absorption spectroscopy, the ability of yttria particles to scavenge 2,2-diphenyl-1-picrylhydrazyl (•DPPH) radicals, was reported [53]. Nevertheless, these particles were synthesized under calcination at high temperatures (such as at 723 K [37], 973 K or 1173 K [53]), of yttrium (III) precursors. This process resulted in agglomerated particles with no control over their size or shape. In addition, up to now, there are no reports evaluating the antioxidant properties of yttria nanoparticles as a function of their sizes and shapes. Furthermore, studies evaluating •OH scavenging properties of yttria nanocrystals via the Fenton assay, are lacking. By analysing the antioxidant properties of yttria particles with this method, would allow for a better comparison with already reported ceria antioxidants.

We evaluated •OH scavenging properties of yttria nanocrystals through the Fenton assay, as a function of their sizes and shapes. Different sizes and shapes of yttria nanocrystals were synthesized by applying wet chemical methodologies, including thermal decomposition and digestive ripening. In addition, we explored the effect of dopants, embedded within the yttria host, on the radical scavenging capacity and compared their antioxidant activity with state of the art ceria nanoparticles. We also performed *ex-vivo* experiments with the goal of determining if yttria can prevent the generation of •OH within biological mediums.

2. Experiments

2.1. Materials

Yttrium acetate hydrate ($Y(CH_3CO_2)_3{\cdot}H_2O$ as $Y(Ac)_3{\cdot}H_2O$, purity 99.99%), erbium acetate tetrahydrate ($Er(CH_3CO_2)_3{\cdot}4\ H_2O$ as $Er(Ac)_3{\cdot}4\ H_2O$, purity 99.99%), oleylamine ($C_{18}H_{35}NH_2$, as OLAM, purity 70%), methyl violet (MV), iron sulfate pentahydrate ($FeSO_4{\cdot}7\ H_2O$), and Tris-HCl buffer (pH=4.5), were purchased from Sigma Aldrich. Ytterbium acetate tetrahydrate ($Yb(CH_3CO_2)_3{\cdot}4\ H_2O$ as $Yb(Ac)_3{\cdot}4\ H_2O$, purity 99.99%), was purchased from Apollo Scientific. Oleic acid ($CH_3(CH_2)_7CH{=}CH(CH_2)_7COOH$, as OLAC, purity 90%), 1-octadecene ($CH_3(CH_2)_{15}CH{=}CH_2$ as ODE, purity 90%), hexane (99%), and sodium nitrate ($NaNO_3$, 99%) were purchased from Alfa Aesar. Sodium chloride (NaCl), H_2O_2 (30 wt%) and ethanol (EtOH) were purchased from Merck and VWR Chemicals, respectively.

2.2. Synthesis of yttrium oxide nanocrystals

Yttria nanocrystals with the shape of branched nanotriangles and irregular particles resembling a heart (hereafter nanohearts), were synthesized via a thermal decomposition method, as previously reported [54]. In a typical synthesis of undoped Y_2O_3 branched nanotriangles, 2.5 mmol of $Y(Ac)_3{\cdot}H_2O$ and 4 mmol of $NaNO_3$ were added to a mixture of 25 mmol OLAC, 25 mmol OLAM and 15 mmol ODE in a three-neck flask. The reaction mixture was degassed at 393 K for 0.5 h to ensure the removal of residual oxygen species and complexation of lanthanide ions with the organic surfactants. After switching to nitrogen atmosphere, the mixture was heated at 583 K and maintained at this temperature for a period of 0.5 h. The reaction was cooled down naturally to room temperature. Purification was conducted through the addition of ethanol, followed by centrifugation at 5000 rpm during 10 min and redispersion of the precipitates in hexane. This purification cycle was repeated three times. For the synthesis of doped nanotriangles, the methodology was the same, except that 2 mol% $Er(Ac)_3{\cdot}4\ H_2O$ and 10 mol% $Yb(Ac)_3{\cdot}4\ H_2O$ (or 4 mol% $Er(Ac)_3{\cdot}4\ H_2O$ and 4 mol% $Yb(Ac)_3{\cdot}4\ H_2O$) substituting partially $Y(Ac)_3{\cdot}H_2O$, were introduced at the beginning of the reaction. For the synthesis of undoped yttrium oxide nanohearts, the methodology was identical, except that the reaction mixture was treated at 583 K for a period of 2 h.

Yttria nanocrystals with the shape of self-assembled nanodiscs were synthesized via a digestive ripening method, adapted with slight modification from a previously reported work [55]. In a typical synthesis, 0.2 mmol $Y(Ac)_3{\cdot}H_2O$, 0.1 mmol of NaCl and 45 mmol of OLAM, were added to a three-neck flask and heated at 553 K using a ramp of 15 K min^{-1} under protective nitrogen atmosphere. At 553 K, 15 mmol of OLAC were swiftly injected in the reaction flask and the reaction mixture was allowed to age for 1 h, prior to cooling down naturally at room temperature. The product of the reaction was extracted by adding ethanol to the solution, followed by centrifugation at 4000 rpm for 10 min, after which the supernatant was discarded, and the precipitate was redissolved in hexane. The purification cycles were repeated until the discarded supernatant was colourless. The final products of all the reactions analysed could be either stored as a dispersion or as a solid powder by evaporating the liquid in a muffle furnace at 333 K for 4 h.

2.3. Preparation of water dispersible yttrium oxide nanocrystals

Water dispersible Y_2O_3 nanocrystals were prepared by treating the as-synthesized particles under acidic conditions, as reported elsewhere [56]. Briefly, 60 mg of the as-synthesized dried nanoparticles were dispersed in 30 mL of a solution of HCl and ethanol with pH adjusted to 1.0. The mixture was sonicated for 1 h. Ligand free nanoparticles were obtained after centrifugation at 6500 rpm for 10 min and washing with a HCl/ethanol solution, with pH adjusted to 4.0. Several washing cycles lead to the final dispersion of these nanoparticles in distilled water.

2.4. Hydroxyl radical scavenging properties

The antioxidant properties of the nanocrystals were analyzed by investigating their capability to scavenge •OH from Fenton reagents in a MV solution. Stock water solutions of MV (1 mM), Tris-HCl buffer (0.5 M), $FeSO_4{\cdot}7\ H_2O$ (0.45 mM), H_2O_2 (2 M) and water dispersions of yttria nanoparticles of different shapes (nanotriangles, nanohearts or nanodiscs with 20 mg mL^{-1} concentration each), were prepared separately before the photometric analysis. A reaction solution with a final volume of 4 mL was prepared, composed of $1.2{\cdot}10^{-5}$ M MV, 0.15 mM $FeSO_4{\cdot}7\ H_2O$, 1.0 M of H_2O_2, 0.1 M Tris-HCl buffer [24,28,29], to which 0.1 to 2 mg mL^{-1} water dispersible yttria nanoparticles were added. These concentrations of the nanoparticles were inspired from similar tests conducted for ceria, a classical antioxidant oxide with a similar structure and properties than yttria [57]. The reaction solution was thoroughly mixed by sonicating it for 5 min prior to the UV–VIS absorbance

measurements using a UV–VIS-NIR Cary 5000 spectrophotometer. All experiments were repeated three times, and the results reported are the average values of these repeated experiments.

2.5. Ex-vivo scavenging properties

For the *ex-vivo* experiments, the decomposition of H_2O_2 by liver catalase and the role of the yttria nanoparticles as antioxidant agents were explored. Within these experiments, an exothermic reaction takes place when liver catalase reacts with H_2O_2, accompanied by the formation of foam [58]. In the experiments we used fresh fat pig liver, distilled water, yttria nanoparticles and H_2O_2.

In a typical *ex-vivo* experiment, different quantities of fresh fat pig liver, distilled water, yttria nanoparticles and H_2O_2, were added in this order. The optimal quantities were evaluated by tracking the reaction solution through absorbance measurements in a UV–VIS-NIR Cary 5000 spectrophotometer, with the goal of observing the evolution of the absorption band of liver catalase, and by recording the temperature within the solution through a platinum and platinum-10% rhodium thermocouple connected to a digital multimeter. Fresh fat pig liver was smashed by a blender. Smashed liver, 70 mg, was dispersed in distilled water (5.5 mL) by sonicating it for a period of 0.5 h. Analysis were acquired within a period of 5 min to avoid flocculation of the smashed liver within the solution. All experiments were repeated three times, and the results reported are the average values of these repeated experiments.

Within the aqueous solution of the smashed liver, we initially tested the effect of different volumes of H_2O_2 and monitored the absorbance of liver. In addition, here an exothermic reaction takes place. The temperature changes within a period of 5 min were recorded using the thermocouple. After that, we tested the effect of the addition of undoped and Er^{3+}, Yb^{3+} codoped yttria nanoparticles on the reaction to analyze their antioxidant properties in this biological system.

2.6. Characterizations

The crystalline structures of the as synthesized and acid treated particles were investigated by X-ray powder diffraction (XRPD). The measurements were made using a Siemens D5000 diffractometer (with Bragg-Brentano parafocusing geometry and a vertical θ-θ goniometer) fitted with a curved graphite diffracted-beam monochromator, incident and diffracted-beam Soller slits, a 0.06° receiving slit, and a scintillation counter as detector. The angular 2θ diffraction range was set between 5° and 70°. The data were collected with an angular step of 0.05° at 3 s per step with sample rotation to increase the statistics of the signal collected. Cu K_α radiation was obtained from a copper X-ray tube operated at 40 kV and 30 mA.

The size and shape of the nanoparticles were investigated by electron microscopy. The images were acquired using a JEOL JEM-1011 transmission electron microscope (TEM) operating at an accelerating voltage of 100 kV. For the preparation of the samples, the nanocrystals were dispersed in hexane (for the as-synthesized nanoparticles), and in distilled water (for the acid treated nanoparticles). Around 7 μL of these dispersions were placed on the surface of a copper grid covered by a holey carbon film (HD200 copper formvar/carbon). Their size distributions were determined using the Image J software after analysing over 100 nanocrystals.

The ligands present on the surfaces of the as-synthesized and acid treated nanoparticles were investigated using Fourier Transform Infrared (FT-IR) spectroscopy. The spectra were recorded in the range of 400–4000 cm^{-1} in a FT-IR IluminatIR II, Smith spectrophotometer.

3. Results and discussion

3.1. Synthesis of yttrium oxide nanocrystals

Yttria nanocrystals of different sizes and shapes were synthesized via wet chemical methodologies, namely thermal decomposition and digestive ripening. Via the thermal decomposition [54], branched nanotriangles (Fig. 1(a), and Fig. S1 at SI) and nanohearts (Fig. 1(b)), were obtained as final products. The branched nanotriangles have an average lateral dimension of 25 ± 2 nm (Fig. 2(a)), whereas the nanohearts are in the range of 35 ± 3 nm (Fig. 2(b)). For the nanocrystals synthesized via the digestive ripening method [55], the shape matches that of self-assembled nanodiscs (Fig. 1(c)), with a mean diameter of 22 ± 7 nm (Fig. 2(c)) and a thickness close to the unit cell dimensions (1 ± 0.1 nm), as determined by the TEM images (Fig. S2 at SI).

In order to make these nanocrystals compatible for radical scavenging assays in biological environments, water dispersible particles were prepared [2]. To achieve this, the as-synthesized nanocrystals, were treated under acidic conditions to remove the capping organic surfactants [56]. The sizes and shapes of the nanocrystals obtained after this treatment were examined by TEM. The acidic treatment substantially affected the shapes of the nanoparticles. For the branched nanotriangles, their shape has changed to an almost irregular one, with the edges totally extinct (Fig. 1(d)). In addition, these nanoparticles tend to agglomerate, probably due to the absence of coating organic surfactants. Concerning the size, they are similar to the as-synthesized nanotriangles, around 26 ± 3 nm (Fig. 2(a)). On the other hand, the shape and sizes (36 ± 10 nm, Fig. 2(b)) of the nanohearts is maintained (Fig. 1(e)), although they also tend to aggregate. Self-assembled nanodiscs display radical changes. It seems that their ability to self-assemble is only maintained due to the presence of oleic acid moieties attached to their surfaces. This is proved by determining the disc-to-disc distance (around 3.8 nm: Fig. S2 at SI) [55,59], which matches with the double of the projected distance of the *cis*-oleic acid molecule [60]. After the acidic treatment, the surfactant is removed from the surface of the nanodiscs, which in turn, disassemble (Fig. 1(f)). As a result, disc shaped particles with average diameters around 7 ± 3 nm are obtained (Fig. 2(c)).

Regardless of the shape and size of the nanocrystals and if they have been treated with acid or not, their crystalline structures match with data described elsewhere [54,55]. In general, the XRPD patterns are composed of broad peaks, attributed to the small sizes of the nanocrystals. In addition, it could be noticed the absence (in the self-assembled nanodiscs) or the presence (in the branched nanotriangles and nanohearts) of the (400) peak, which indicates the crystallographic orientation of the observed morphologies [54,55]. For the branched nanotriangles and nanohearts, the planes are aligned perpendicular to the [400] direction [54], whereas for the self-assembled nanodiscs, the orientation is towards the [100] direction [55].

We also analyzed the ligands attached to the surface of the yttria nanocrystals by FT-IR. The as-synthesized nanocrystals show the presence of oleic acid moieties on their surfaces. Oleic acid does not appear in its pure form, confirmed by the absence of the characteristic band of the -C═O stretching mode usually located at 1710 cm^{-1}. This band is replaced by bands appearing at 1580 cm^{-1} and 1435 cm^{-1} for the branched nanotriangles and nanohearts. On the other hand, for the self-assembled nanodiscs, bands at 1605 cm^{-1} and 1420 cm^{-1} (yellow lines in Fig. 3(b)), are appearing. These bands are ascribed to the antisymmetric and symmetric stretching vibrations of the deprotonated carboxylic group (COO^-) [61]. This is an indication that OLAC molecules were deprotonated into carboxylates anions due to the promotion of OLAM [61]. The absence of OLAM is expected, as the role of this surfactant is to catalyze the deprotonation of OLAC [62]. This observation is in line with other articles that confirm that no FT-IR spectral features characteristics of an amine-containing species are detected [61,63,64], even when in the reaction only OLAM is employed [65]. The peaks at 2850 and 2924 cm^{-1} are assignable to the symmetric and the antisymmetric methylene group stretches (ν_s (-CH_2) and (ν_{as} (-CH_2)) of OLAC [64,66]. A very weak shoulder around 2924 cm^{-1} is assigned to the antisymmetric methyl stretch ν_{as} (-CH_3).

For the particles treated under acidic conditions, the FT-IR spectrum

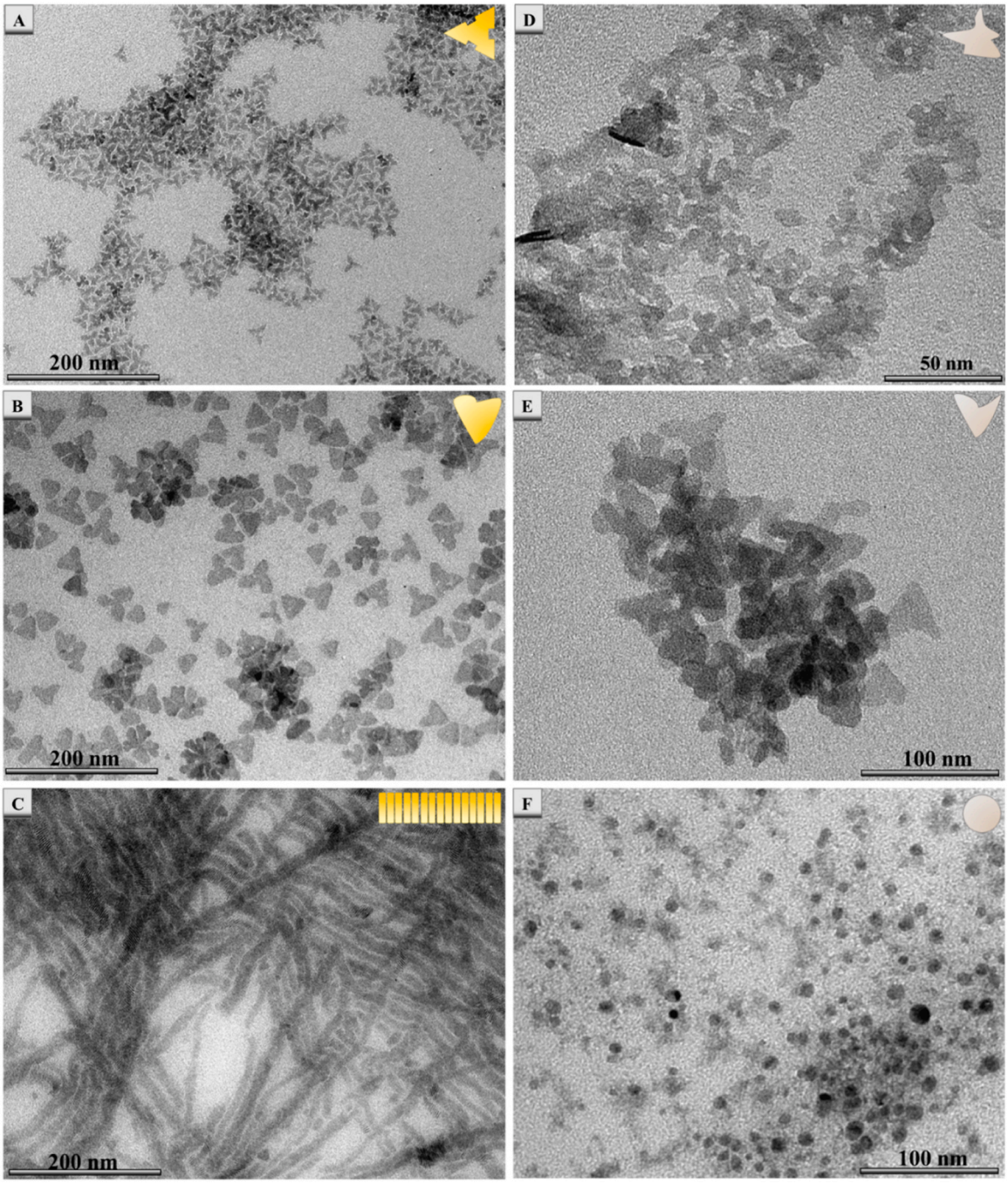

Fig. 1. TEM images of as-synthesized and acid treated Y_2O_3 nanoparticles: (a), (d) branched nanotriangles, (b), (e) nanohearts, and (c), (f) nanodiscs.

reveals that the intensity of most of these bands are weakened. For example, the shoulder band at around 2924 cm^{-1} and 2850 cm^{-1} or the carboxylate bands at 1580 cm^{-1} and 1435 cm^{-1} have decreased (gray dotted lines in Fig. 3(b)). The weakening of the organic ligand bands is in accordance with what has been observed in the acidic treatment of other types of nanoparticles, capped with oleic acid moieties such as $NaYF_4$ [56], Mn_3O_4 [67], and Fe_3O_4 nanoparticles [68]. In addition, the appearance of a broad band around 3400 cm^{-1} is detected. It is assigned to the O-H stretching band of water [69]. These results confirm that we modified the surface of the nanoparticles to facilitate their dispersibility in water.

3.2. *Hydroxyl radical scavenging properties of yttrium oxide nanocrystals*

The antioxidant properties of water dispersible yttria nanocrystals were determined by their ability to scavenge •OH produced in the Fenton assay, using MV as a chromogenic agent. In this assay, the decomposition of H_2O_2 in the presence of metal ions such as Cu^+ or Fe^{2+}, leads to the generation of •OH [2,70,71]. The result of this reaction is reflected by a decoloration of MV solution, since MV, dissolved in water, displays a purple color with a maxim absorbance located at 590 nm [72]. The Fenton reagents, Fe^{2+} and H_2O_2 under acidic, neutral or basic conditions [24,70,71,73], can react to generate •OH. These radicals can quickly interact with MV by attacking its –C═C– bond, oxidizing the purple MV into colorless MV [24,70,71,73]. This oxidation process is manifested by a decrease of the absorbance of MV [13,28,29]. When the

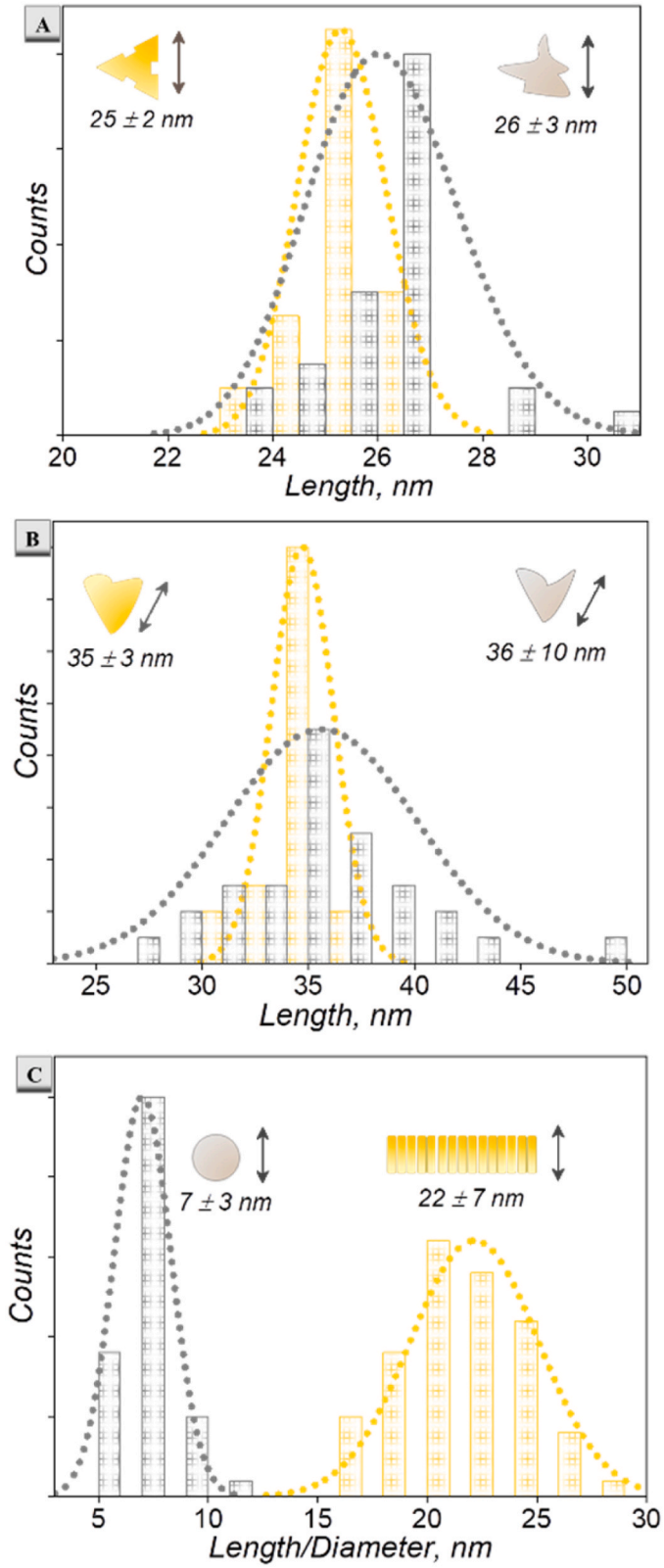

Fig. 2. Size distribution of as-synthesized (in yellow) and acid treated (in gray) Y_2O_3 nanoparticles: (a) branched nanotriangles, (b) nanohearts, and (c) nanodiscs.

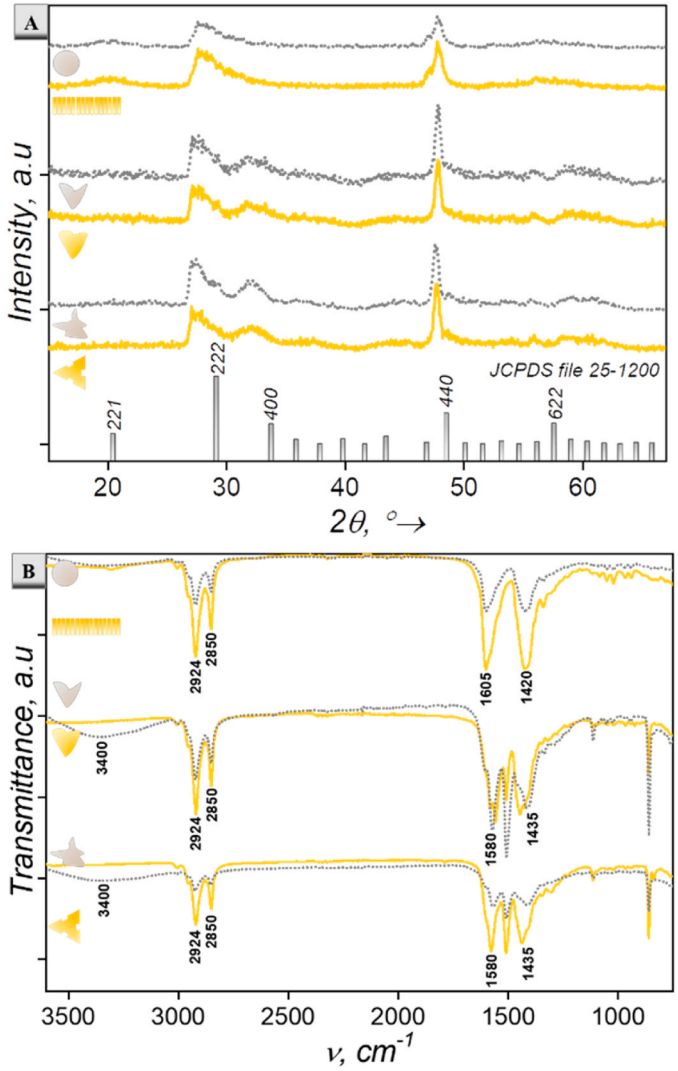

Fig. 3. (a) XRPD and (b) FT-IR of as-synthesized (in yellow) and acid treated (in grey) Y_2O_3 nanoparticles. The reference card of cubic Y_2O_3 (JCPDS 25–1200) is included for comparison.

antioxidant agent is added, it prevents the decoloration MV solution by scavenging •OH. This reaction is easy followed by optical absorption spectroscopy [2,70,71].

The ability of yttria nanocrystals to prevent the degradation of MV from •OH is monitored via optical absorption spectroscopy. For the UV-Vis experiments, first, we determined the absorbance of MV, dispersed in distilled water with a concentration of $1.2{\cdot}10^{-5}$ M, as a function of time. Results reveal that, within a time frame of at least 30 min, long enough to perform the Fenton reaction, no change in the absorbance of MV could be detected (Fig. S3 (a) at SI). Then, a new solution containing MV, H_2O_2 (1 M concentration) and Y_2O_3 (nanotriangles with a concentration 0.1 mg mL^{-1}), in the absence of the Fenton reagents, was prepared and the absorbance was measured. No differences were observed with respect to MV in distilled water only (Fig. S3 (b) at SI), indicating that in the absence of Fe^{2+} ions, the Fenton reaction cannot take place, and thus, •OH could not be generated.

When Fe^{2+} ions are added to a new solution with MV, H_2O_2 and Y_2O_3 (same concentrations as above), the Fenton reaction takes place and •OH can be generated within the medium. Fig. 4(a) displays the comparison of the absorbance spectra of a solution containing only MV in distilled water (purple line), a solution containing MV, Fe^{2+} ions at a 0.15 mM concentration, and H_2O_2 at a 1 M concentration (Fenton

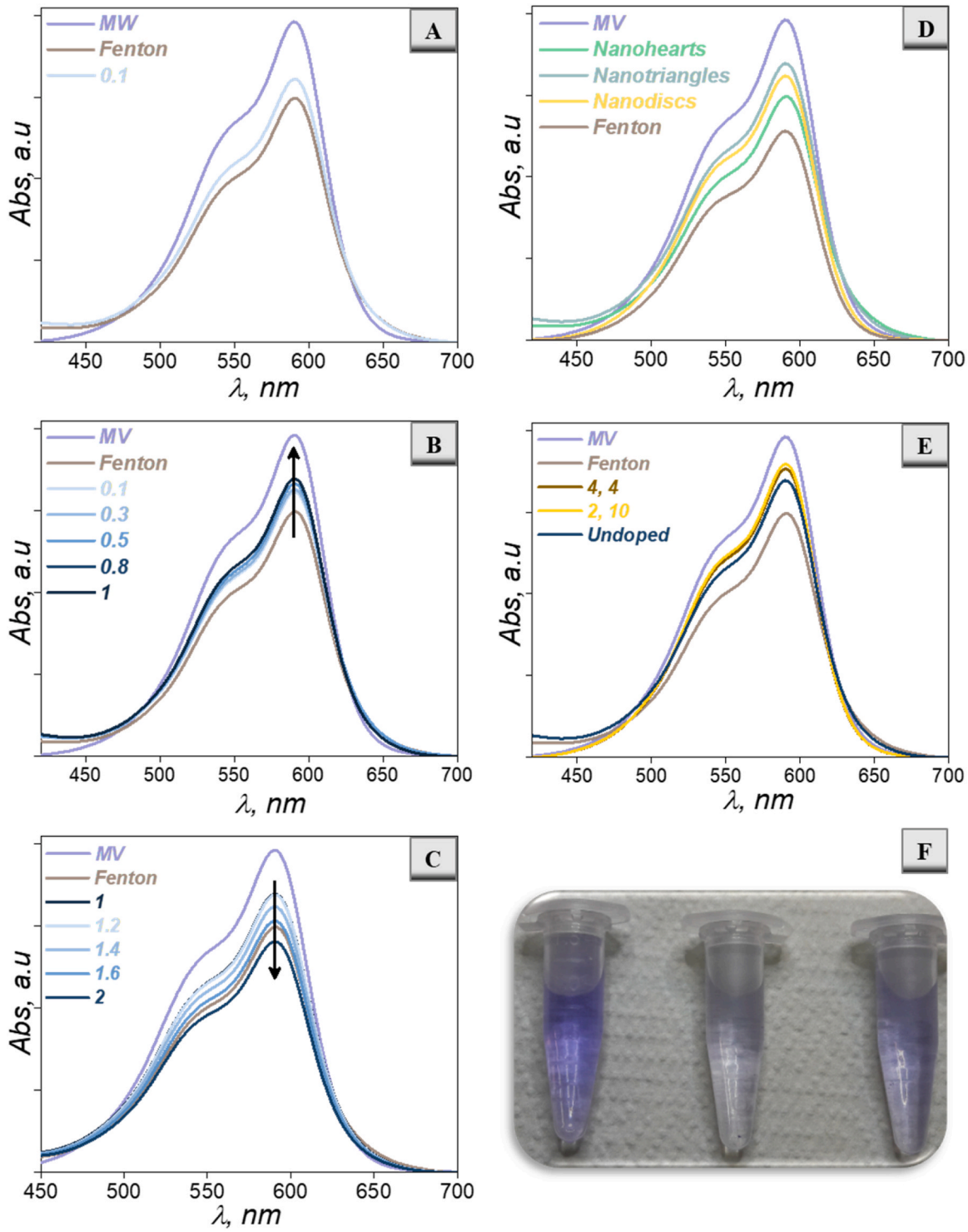

Fig. 4. Absorbance spectra of methyl violet: (a) in distilled water, in the Fenton reaction solution, and with the addition of yttria nanoparticles; (b) tuning the concentration of yttria nanoparticles in the Fenton reaction from 0.1 mg mL^{-1} to 1 mg mL^{-1}; (c) tuning the concentration of yttria nanoparticles in the Fenton reaction from 1 mg mL^{-1} to 2 mg mL^{-1}; (d) tuning the morphology of yttria nanoparticles (nanotriangles with average sizes of 26 ± 3 nm, nanohearts with average sizes of 36 ± 10 nm and nanodiscs with an average diameter of 7 ± 3 nm; (e) doping ions incorporated in the yttria nanotriangles(4 mol% Er^{3+}, 4 mol% Yb^{3+} and 2 mol% Er^{3+}, 10 mol% Yb^{3+}). (f) Pictures displaying the change in color of the methyl violet in distilled water (left), in the Fenton reaction solution without the nanoparticles (middle) and with 2 mol% Er^{3+}, 10 mol% Yb^{3+} doped yttria nanotriangles (right).

reaction in brown line), and a Fenton reaction solution to which yttria nanotriangles were added with a concentration of 0. 1 mg mL^{-1} (blue line), inspired from previously reported investigations on ceria [13,24, 29]. The incubation time in all scenarios has been less than 2 min. Clearly, a decrease in the intensity of the peak of maximum absorbance after the Fenton reaction was observed, suggesting that MV molecules have been oxidized. When yttria nanoparticles are introduced into the solution, the intensity of the absorbance recovers part of its value. These results show the ability of our yttria nanoparticles to scavenge part of •OH and protect MV from further oxidation.

It has been recently reported that several factors can significantly affect the antioxidant activity of the nanocrystals [74]. One of these factors is the concentration of nanocrystals added in the reaction. Lu *et al.*[74] found that when increasing the concentration of ceria nanoparticles up to 20 μM, the antioxidant properties exhibited by these nanoparticles are improved. Nevertheless, an additional increase of the concentration until 50 μM lead to the disappearance of the antioxidant properties, and instead, an enhancement of the oxidant activity was observed [74]. Following this idea, we tuned the concentration of yttria nanotriangles to determine which concentration scavenged most effectively the formation of •OH in the Fenton reaction.

Results reveal that the antioxidant properties of Y_2O_3 nanoparticles depend on their concentration (Fig. 4(b), (c)). For concentrations up to 1 mg mL^{-1}, their capacity to prevent the generation of •OH increases, achieving a maximum for a concentration of 1 mg mL^{-1} (Fig. 4(b)). Instead, a further increase of the concentration up to 2 mg mL^{-1}, causes a decrease in the antioxidant activity of the nanoparticles (Fig. 4(c)) until they disappear totally, and further oxidation of MV is observed. Thus, a concentration of 1 mg mL^{-1} seems to be the optimal concentration to maximize the antioxidant activity of the yttria nanotriangles.

We also analyzed the effect of the shape and size of the yttria nanoparticles on their antioxidant properties, fixing their concentrations to 1 mg mL^{-1}. Distorted nanotriangles exhibited better antioxidant properties compared with the other morphologies (Fig. 4(d)). Nanohearts exhibited the smallest antioxidant capacity. We believe this can be related to the surface area of the particles. Another possibility is that they are related to the presence of oxygen vacancies in these yttria particles. Despite we did not determine the concentration of oxygen vacancies in our nanocrystals, it is generally accepted that irregular nanocrystals tend to accumulate more oxygen vacancy defects on their surfaces [2,28], which in turn would increase the scavenging of •OH.

Having established nanotriangles as the best antioxidant agent among the yttria nanocrystals synthesized, we finally analyzed if the incorporation of lanthanide dopants in the nanoparticles plays any role on the antioxidant properties exhibited by them. It has been reported that yttria can incorporate lanthanide ions as dopants within its structure replacing Y^{3+} ions [38–44]. Additionally, other studies suggest that the introduction of lanthanide dopants in ceria nanoparticles can enhance their antioxidant properties [13,27].

We tested the antioxidant properties of Er^{3+} and Yb^{3+} co-doped yttria nanotriangles. The doped particles were synthesized through the same thermal decomposition method, and no changes were observed in the crystalline structure (Fig. S4 (a) at SI). However, when comparing the morphology of the undoped and doped nanocrystals, clearly, for the doped ones, slight distortions from the general branched nanotriangle shape, are detected (Fig. S4 (b) at SI), suggesting that dopants can induce irregularities in shape. We explored two different doping concentrations, 4 mol% Er^{3+}, 4 mol% Yb^{3+} and 2 mol% Er^{3+}, 10 mol% Yb^{3+}. It has been reported that dopants can generate also changes in the lattice constants of the host matrices, leading to an increase of the concentration of oxygen vacancies, causing eventually an enhancement of their antioxidant properties [13,27,34]. Indeed, we observed an increase of the antioxidant properties of the Er^{3+} and Yb^{3+} doped yttria nanotriangles when compared to the undoped ones, and these antioxidant properties were slightly better when the quantity of dopants was higher (Fig. 4(e)). The ability of these particles to prevent the degradation of MV could be easily detected by naked eye. Fig. 4(f) shows a picture of a MV solution before the Fenton reaction (left), when the Fenton reaction takes place without adding yttria particles (middle) and when the Fenton reaction takes place in the presence of yttria particles (right).

To compare the antioxidant performance of our yttria nanoparticles with that of ceria nanoparticles, we considered the comparison between the maximum intensity of the absorption band of MV under the different reaction conditions, as previously proposed [74]. Taking as reference the value of the maximum intensity of the absorption band of MV in distilled water, ΔA is defined as the drop in the intensity of this peak under the Fenton reaction conditions (Fig. 5(a)). From another side, Δa corresponds to the decrease in the intensity of this peak when the antioxidant particles are added to the solution (Fig. 5(a)). Then, the evaluation of the performance of the nanoparticles as antioxidant agents is based on the ratio between Δa and ΔA [29,74]. If the nanoparticles can prevent the formation of •OH, the value of Δa should be smaller than ΔA [29,74]. Therefore, the smaller the value of this ratio, the stronger the •OH scavenging properties of the nanocrystals [29,74].

Fig. 5(b) depicts the values of $\Delta a/\Delta A$ ratio for our yttria nanoparticles, together with that of ceria nanoparticles extracted from literature. Several conclusions can be drawn. First, doped nanoparticles, including 2 mol% Er^{3+}, 10 mol% Yb^{3+} and 4 mol% Er^{3+}, 4 mol% Yb^{3+} doped yttria, and 10 mol% lanthanum (La^{3+}) doped ceria [13], exhibit lower values for this ratio, i.e. better antioxidant properties, compared to the corresponding undoped particles. Hence, the use of doped ceria or

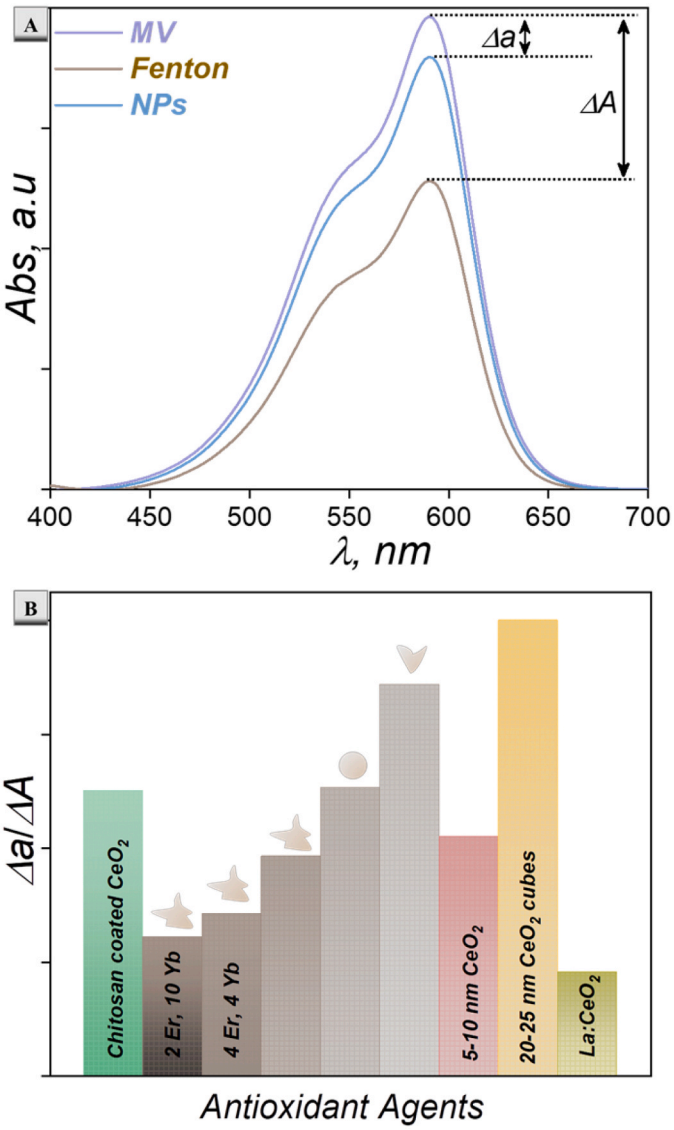

Fig. 5. (a) The model for the determination of the antioxidant capacity of the nanocrystals by considering the changes in the maximum of absorbance for MV, using as an example 2 mol% Er^{3+},10 mol% Yb^{3+} doped yttria nanotriangles. (b) Data chart displaying the antioxidant performance of the different nanocrystals based on the ratio between Δa and ΔA. On the data chart are included yttria based nanocrystals produced within this study showed with their corresponding shapes, and cerium oxide nanocrystals: 5–10 nm CeO_2 nanoparticles and 20–25 nm CeO_2 nanocubes [74], chitosan coated CeO_2 nanoparticles [57], and 10 mol% lanthanum (La) doped ceria nanocubes [13].

yttria nanoparticles can be highlighted as a promising strategy for the future development of antioxidant nanoagents with improved performance. Second, the geometrical characteristics of the antioxidant nanoparticles, such as their sizes and shapes, greatly influence their performance. Smaller particles seem to exhibit better performances (the values of the $\Delta a/\Delta A$ ratio in Fig. 5(b) for 5–10 nm CeO_2 nanoparticles and 20–25 nm CeO_2 nanocubes [74], with the former one being more effective). This might be related to the surface exposed of the nanoparticles. Third, it can be also derived from the data provided in Fig. 5 (b), that coating the particles with biocompatible molecules as chitosan, can affect the antioxidant properties, reducing them, probably because the active sites of the antioxidant nanoparticles are hampered by the presence of these coating molecules [25,34]. Forth and main conclusion, yttria nanoparticles exhibit similar antioxidant properties with those reported previously for ceria nanoparticles, opening the door for further development of yttria nanoparticles as potential antioxidant agents, for example in biomedical applications.

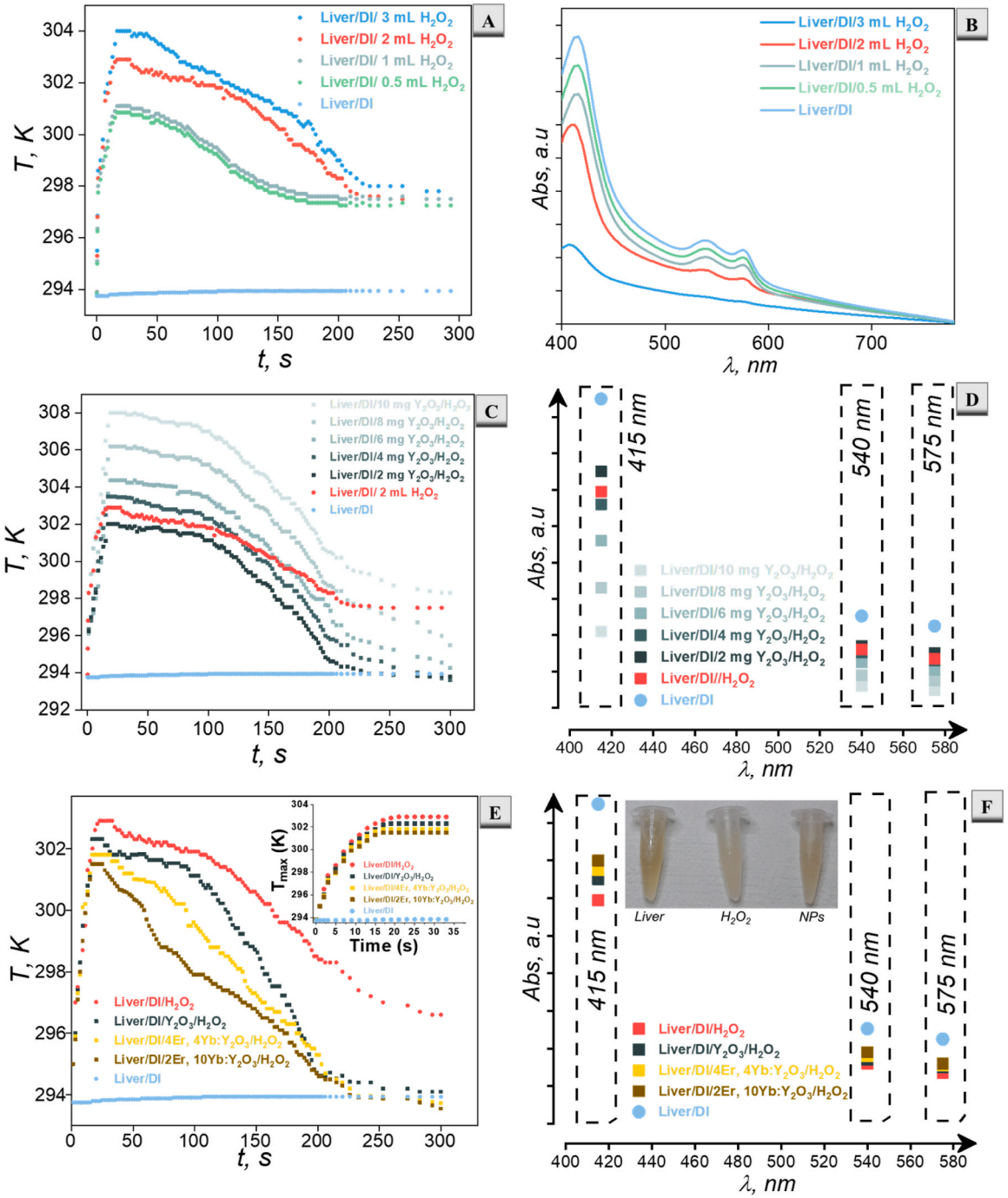

Fig. 6. Absorbance (scattered point of the maximum absorbance for each band in (e) and (f)) and temperature profiles recorded in a solution composed of liver and: (a) and (b) distilled water and different quantities of H_2O_2; (c) and (d) distilled water, 2 mL H_2O_2 and different quantities of undoped yttria nanotriangles; and (e) and (f) distilled water, 2 mL H_2O_2, 2 mg of Er^{3+} and Yb^{3+} doped yttria nanotriangles with different concentrations. The corresponding insets display the maximum temperature reached for the nanoparticles within the first 30 s of the reactions (in (e)) and pictures showing the different colors of the solutions of liver in DI (labelled "*Liver*"); DI and H_2O_2 (labelled "H_2O_2"); DI, Y_2O_3 and H_2O_2 (labelled "*NPs*") (in (f)), respectively.

3.3. Ex-vivo antioxidant properties of yttrium oxide nanocrystals

To demonstrate the applicability of yttria nanocrystals as antioxidant agents in fields related to biosciences, we designed an *ex-vivo* experiment to monitor the reaction of the catalase enzyme, that can be encountered in liver, with hydrogen peroxide. Yttria nanocrystals have been shown to be relatively nontoxic for cultured cells and able to protect nerve cells from oxidative stress caused by exogeneous glutamic acid [35], thus, this justifies their potential use in biological systems.

Catalase consists of a tetramer of four polypeptide chains, each over 500 amino acids long, with four iron-containing heme groups [75]. When H_2O_2 enters in contact with liver, an exothermic chemical reaction, followed by the creation of foams, occurs, leading to the generation of oxygen and water molecules [58]. This reaction is promoted by the catalase enzyme. Hence, catalase can eliminate H_2O_2 either by promoting a reaction between two H_2O_2 molecules resulting in the formation of water and oxygen, or by promoting the interaction of H_2O_2 with compounds such as alcoholic beverages that serve as hydrogen donors, so that H_2O_2 can be converted to one molecule of water, and the reduced donor becomes oxidized (a process called the peroxidic activity of catalase) [12,58]. Hence, this enzyme prevents the generation of •OH within the liver. We underline the similarities between the reactions of Fe^{2+} in the Fenton assay with the one of catalase with H_2O_2. In both reactions, the presence of Fe^{2+} allows for the generation of •OH. Thus, the reaction of catalase with H_2O_2 mimics the Fenton assay.

The goal of the *ex-vivo* experiment was to investigate the antioxidant properties of yttria nanocrystals on the reaction of liver catalase with H_2O_2. If yttria nanocrystals do exhibit antioxidant properties within this biological system, the heat released by the interaction of catalase with H_2O_2 during the experiment, will be reduced compared to the reaction in the absence of these nanoparticles. The reaction was also monitored through spectrophotometric analysis.

In a solution of smashed pork liver in distilled water, different amounts of H_2O_2 were added, and both the absorbance of the dispersion and the temperature generated during the exothermic reaction were monitored to analyze the evolution of the reaction. To obtain substantial enough changes in both parameters to monitor the potential activity of the antioxidant nanoparticles in the subsequent experiments, 2 mL of H_2O_2 had to be added to the solution. Smaller amounts of H_2O_2 generated a change in temperature too small to see any effect from the antioxidant nanoparticles (Fig. 6(a)), while bigger amounts of H_2O_2 cause the absorption bands of catalase to disappear (Fig. 6(b)). We also monitored the temperature in the dispersion of liver only in distilled water as a control experiment. The temperature within this solution remained constant for a monitored period of 5 min. Thus, the increase of temperature observed occurs only when the reaction of liver catalase with H_2O_2 takes place. In addition, to obtain a good spectrum of absorbance of the smashed pork liver in distilled water it was necessary to generate a dispersion of 70 mg of smashed liver in 5.5 mL of distilled water. In this dispersion, we were able to properly record three absorbance bands, located at 415 nm, 540 nm and 575 nm (Fig. 6(b)). The 415 nm band is the so-called Soret band and is assigned to the π-π * transition of the porphyrin hosting iron band. The bands located at 540 nm and 575 nm are attributed to metal-to-ligand charge transfer processes [76]. When yttria nanotriangles were added to the solution, in the sequence: 70 mg liver, 5.5 mL of distilled water, undoped yttria nanotriangles (from 2 mg to 10 mg) and 2 mL of H_2O_2, the antioxidant effect of the yttria nanoparticles could be analyzed. The temperature changes allowed us to monitor more precisely what is happening in the solution for the different quantities of yttria nanoparticles added. When 4 to 10 mg of yttria nanotriangles were added, the temperature of the solution is similar or increased above the temperature recorded in the reaction without the presence of the yttria particles (Fig. 6(c)). Thus, this would imply that at these quantities, the yttria nanocrystals act as an oxidant.

Only when 2 mg of yttria nanoparticles were added, the antioxidant properties were manifested, as the temperature decreased to 302 K, below the temperature obtained only with H_2O_2, around 303 K (Fig. 6 (c)). Fig. 6(d) shows the maximum absorbance of catalase at 415 nm, 540 nm and 575 nm band as a function of the different amount of undoped particles. Only in solutions with a content of 2 mg of yttria nanoparticles, the intensity of the absorption bands increased slightly. The spectra from which these data were extracted can be found in Fig. S5. For higher concentrations of yttria nanoparticle, the absorbance of the catalase decreased, even below the level reached in absence of yttria nanoparticles, probably because at these concentrations, oxidant properties might manifest instead of the antioxidant's ones. Hence, we established 2 mg nanotriangles as the optimal amount of yttria nanoparticles to be added into the solution mixture to reduce the effects of the reaction between catalase and H_2O_2.

Finally, when we introduced Er^{3+} and Yb^{3+} as dopants in the yttria nanoparticles, since the doped yttria nanoparticles exhibited better antioxidant properties in the Fenton assay than the undoped ones, we observed that the temperature increase is lower than when undoped nanoparticles where used (Fig. 6(e)). Among the doped nanoparticles, the highest temperature reached for the 4 mol% Er^{3+}, 4 mol% Yb^{3+} yttria nanoparticles is ~301.5 K, whereas for the 2 mol% Er^{3+}, 10 mol% Yb^{3+} doping concentration is ~301 K. The inset of Fig. 6(e) displays the maximum temperature reached for the nanoparticles within the first 30 s of the reactions). These temperatures are 0.5 and 1 K lower than the temperature achieved with the undoped nanotriangles (Fig. 6(c)). These results seem to demonstrate that the increase of the doping concentration favors the antioxidant properties in these particles. The temperature profile of the doped nanoparticles also decreases faster when compared to that of the undoped nanoparticles (Fig. 6(e)). This indicates that the process of reducing the effects of the reaction between catalase and H_2O_2 develops faster using these nanoparticles, and the liver recovers its normal temperature faster. These results were corroborated by recording the recovery of the intensity of the absorption bands of catalase observed when doped yttria nanoparticles are added to the reaction (Fig. 6(f). In addition, in the inset of Fig. 6(f), it can be observed a photograph showing the different colors of the smashed liver in distilled water (labelled as "*Liver*"), in distilled water and H_2O_2 (labelled as "*H_2O_2*"), and in distilled water, 2 mol% Er^{3+} and 10 mol% Yb^{3+} doped yttria particles and H_2O_2 (labelled as "*NPs*"), highlighting the antioxidant properties of these particles when introduced within this *ex-vivo* system.

Thus, we can conclude that the yttria nanoparticles we developed here might be implemented as antioxidant nanoagents within biological media, catalyzing in this way the elimination of hydrogen peroxide molecules from the medium and preventing the formation of harmful ROS.

4. Conclusions

Yttria nanoparticles display antioxidant properties by scavenging •OH, both in biological and non-biological media. Their antioxidant properties depend on their sizes, shapes, concentrations, and presence of doping lanthanide ions. Yttria nanotriangles, nanohearts and nanodiscs, synthesized via wet chemical methodologies, were tested. First, a concentration of 1 mg mL^{-1} was established for improved antioxidant properties. At this concentration, among the three types of nanoparticles, nanotriangles displayed better antioxidant performance on scavenging •OH. The introduction of dopants, such as Er^{3+} and Yb^{3+} and their concentrations, also influenced the ability to scavenge •OH. The antioxidant properties are enhanced with the introduction of dopants at larger concentrations. These antioxidant properties match the current state of the art ceria nanoparticles. These yttria particles can scavenge •OH also in *ex-vivo* media, opening in this way possible applications of the particles in biomedical fields. As future directions, a general optimization of the concentration dependent antioxidant properties should be performed [74]. In addition, the lanthanide ions added as dopants,

could be used to build luminescent thermometers [77,78], to monitor the increase of temperature during the *ex-vivo* experiments [43,44], allowing for the development of a self-assessed antioxidant agent. Within this work, the low concentration of particles added into the *ex-vivo* experiments, hampers the observation of visible emissions arising from these ions.

CRediT authorship contribution statement

Díaz Francesc: Funding acquisition. **Pujol Maria Cinta:** Conceptualization, Supervision, Writing – review & editing. **Aguiló Magdalena:** Funding acquisition. **Carvajal Joan Josep:** Conceptualization, Supervision, Writing – review & editing. **Nexha Albenc:** Conceptualization, Data curation, Investigation, Methodology, Writing – original draft.

Declaration of Competing Interest

The authors declare that they have no known competing financial interests or personal relationships that could have appeared to influence the work reported in this paper.

Data availability

Data will be made available on request.

Acknowledgements

This work was supported by the Spanish Government under projects MAT2016–75716-C2–1-R (AEI/FEDER, UE) and by the Generalitat de Catalunya under project 2017SGR755. A.N acknowledges financial support from the Generalitat de Catalunya under grant 2017FI_B00620, 2018FI_B100161 and 2019FI_B200154.

Appendix A. Supporting information

Supplementary data associated with this article can be found in the online version at doi:10.1016/j.jallcom.2024.173565.

References

[1] A. Orient, Á. Donkó, A. Szabó, T.L. Leto, M. Geiszt, Novel sources of reactive oxygen species in the human body, Nephrol. Dial. Transplant. 22 (2007) 1281–1288.
[2] L. Valgimigli, A. Baschieri, R. Amorati, Antioxidant activity of nanomaterials, J. Mater. Chem. B 6 (2018) 2036–2051.
[3] Y. Fan, G. Huang, Preparation, structural analysis and antioxidant activity of polysaccharides and their derivatives from Pueraria lobata, Chem. Biodivers. 20 (2023) e202201253.
[4] B. Lin, Y. Fan, G. Huang, Preparation, analysis and properties of shaddock ped polysaccharide and its derivatives, Carbohydr. Res. 533 (2023) 108932.
[5] B. Lin, S. Wang, A. Zhou, Q. Hu, G. Huang, Ultrasound-assisted enzyme extraction and properties of shatian pomelo peel polysaccharide, Ultrason. Sonochem. 98 (2023) 106507.
[6] W. Zhang, W. Duan, G. Huang, H. Huang, Ultrasonic-assisted extraction, analysis and properties of mung bean peel polysaccharide, Ultrason. Sonochem. 98 (2023) 106487.
[7] J. Cadet, J.R. Wagner, Oxidatively generated base damage to cellular DNA by hydroxyl radical and one-electron oxidants: similarities and differences, Arch. Biochem. Biophys. 557 (2014) 47–54.
[8] T. Finkel, M. Serrano, M.A. Blasco, The common biology of cancer and ageing, Nature 448 (2007) 767–774.
[9] J. Morry, W. Ngamcherdtrakul, W. Yantasee, Oxidative stress in cancer and fibrosis: opportunity for therapeutic intervention with antioxidant compounds, enzymes, and nanoparticles, Redox Biol. 11 (2017) 240–253.
[10] S.G. Rhee, H_2O_2, a necessary evil for cell signaling, Science 312 (2006) 1882–1883.
[11] H.D. Scheibmeir, K. Christensen, S.H. Whitaker, J. Jegaethesan, R. Clancy, J. D. Pierce, A review of free radicals and antioxidants for critical care nurses, Intensive Crit. Care Nurs. 21 (2005) 24–28.
[12] D. Wu, A. Cederbaum, Alcohol, oxidative stress, and free radical damage, Alcohol Res. Health 27 (2003) 277–284.
[13] S. Fernandez-Garcia, L. Jiang, M. Tinoco, A.B. Hungria, J. Han, G. Blanco, J. J. Calvino, X. Chen, Enhanced hydroxyl radical scavenging activity by doping lanthanum in ceria nanocubes, J. Phys. Chem. C. 120 (2016) 1891–1901.
[14] D. Sorriento, N. De Luca, B. Trimarco, G. Iaccarino, The antioxidant therapy: new insights in the treatment of hypertension, Front. Physiol. 9 (2018) 258.
[15] C.K. Davis, R. Vemuganti, Antioxidant therapies in traumatic brain injury, Neurochem. Int. 152 (2022) 105255.
[16] P.K.J.P.D. Wanasundara, F. Shahidi, Antioxidants: Science, Technology, and Applications, in: Bailey's Industrial Oil and Fat Products.
[17] C.E. Boozer, G.S. Hammond, C.E. Hamilton, J.N. Sen, Air oxidation of hydrocarbons.1 II. The stoichiometry and fate of inhibitors in benzene and chlorobenzene, J. Am. Chem. C. 77 (1955) 3233–3237.
[18] A. Karakoti, S. Singh, J.M. Dowding, S. Seal, W.T. Self, Redox-active radical scavenging nanomaterials, Chem. Soc. Rev. 39 (2010) 4422–4432.
[19] D. Das, B.C. Nath, P. Phukon, S.K. Dolui, Synthesis and evaluation of antioxidant and antibacterial behavior of CuO nanoparticles, Colloid. Surf. B Biointerfaces 101 (2013) 430–433.
[20] S. Paul, J.P. Saikia, S.K. Samdarshi, B.K. Konwar, Investigation of antioxidant property of iron oxide particlesby 1′-1′diphenylpicryl-hydrazyle (DPPH) method, J. Magn. Magn. Mater. 321 (2009) 3621–3623.
[21] J.P. Saikia, S. Paul, B.K. Konwar, S.K. Samdarshi, Nickel oxide nanoparticles: a novel antioxidant, Colloids Surf. B Biointerfaces 78 (2010) 146–148.
[22] N. Singh, M.A. Savanur, S. Srivastava, P. D'Silva, G. Mugesh, A redox modulatory Mn_3O_4 nanozyme with multi-enzyme activity provides efficient cytoprotection to human cells in a Parkinson's disease model, Angew. Chem. Int. Ed. 56 (2017) 14267–14271.
[23] N.J. Abuid, K.M. Gattás-Asfura, E.A. Schofield, C.L. Stabler, Layer-by-layer cerium oxide nanoparticle coating for antioxidant protection of encapsulated beta cells, Adv. Healthc. Mater. 8 (2019) 1801493.
[24] T.J. Fisher, Y. Zhou, T.S. Wu, M. Wang, Y.L. Soo, C.L. Cheung, Structure-activity relationship of nanostructured ceria for the catalytic generation of hydroxyl radicals, Nanoscale 11 (2019) 4552–4561.
[25] S.S. Lee, W. Song, M. Cho, H.L. Puppala, P. Nguyen, H. Zhu, L. Segatori, V. L. Colvin, Antioxidant properties of cerium oxide nanocrystals as a function of nanocrystal diameter and surface coating, ACS Nano 7 (2013) 9693–9703.
[26] R.N. Mitra, M.J. Merwin, Z. Han, S.M. Conley, M.R. Al-Ubaidi, M.I. Naash, Yttrium oxide nanoparticles prevent photoreceptor death in a light-damage model of retinal degeneration, Free Radic. Biol. Med. 75 (2014) 140–148.
[27] A. Olvera Salazar, M. García Hernández, P.Y. López Camacho, A. López Marure, A. I. Reyes de la Torre, Á.d.J. Morales Ramírez, F. Hernández Santiago, L. Aguilera Vázquez, Influence of Eu^{3+} doping content on antioxidant properties of Lu_2O_3 sol-gel derived nanoparticles, Mater. Sci. Eng. C, 69 (2016) 850–855.
[28] Y.J. Wang, H. Dong, G.M. Lyu, H.Y. Zhang, J. Ke, L.Q. Kang, J.L. Teng, L.D. Sun, R. Si, J. Zhang, Y.J. Liu, Y.W. Zhang, Y.H. Huang, C.H. Yan, Engineering the defect state and reducibility of ceria based nanoparticles for improved anti-oxidation performance, Nanoscale 7 (2015) 13981–13990.
[29] Y. Xue, Q. Luan, D. Yang, X. Yao, K. Zhou, Direct evidence for hydroxyl radical scavenging activity of cerium oxide nanoparticles, J. Phys. Chem. C. 115 (2011) 4433–4438.
[30] J. Chen, S. Patil, S. Seal, J.F. McGinnis, Rare earth nanoparticles prevent retinal degeneration induced by intracellular peroxides, Nat. Nanotechnol. 1 (2006) 142–150.
[31] J. Colon, L. Herrera, J. Smith, S. Patil, C. Komanski, P. Kupelian, S. Seal, D. W. Jenkins, C.H. Baker, Protection from radiation-induced pneumonitis using cerium oxide nanoparticles, Nanomed. Nanotechnol. Biol. Med. 5 (2009) 225–231.
[32] G. Fernández-Varo, M. Perramón, S. Carvajal, D. Oró, E. Casals, L. Boix, L. Oller, L. Macías-Muñoz, S. Marfà, G. Casals, M. Morales-Ruiz, P. Casado, P.R. Cutillas, J. Bruix, M. Navasa, J. Fuster, J.C. Garcia-Valdecasas, M.C. Pavel, V. Puntes, W. Jiménez, Bespoken nanoceria: an effective treatment in experimental hepatocellular carcinoma, Hepatology (72 () (2020).
[33] J. Niu, A. Azfer, L.M. Rogers, X. Wang, P.E. Kolattukudy, Cardioprotective effects of cerium oxide nanoparticles in a transgenic murine model of cardiomyopathy, Cardiovasc. Res. 73 (2007) 549–559.
[34] H. Dong, S.R. Du, X.Y. Zheng, G.M. Lyu, L.D. Sun, L.D. Li, P.Z. Zhang, C. Zhang, C. H. Yan, Lanthanide nanoparticles: from design toward bioimaging and therapy, Chem. Rev. 115 (2015) 10725–10815.
[35] D. Schubert, R. Dargusch, J. Raitano, S.W. Chan, Cerium and yttrium oxide nanoparticles are neuroprotective, Biochem. Biophys. Res. Commun. 342 (2006) 86–91.
[36] A. Khurana, P. Anchi, P. Allawadhi, V. Kumar, N. Sayed, G. Packirisamy, C. Godugu, Yttrium oxide nanoparticles reduce the severity of acute pancreatitis caused by cerulein hyperstimulation, Nanomed. Nanotechnol. Biol. Med. 18 (2019) 54–65.
[37] S. Kassem, M. Mohamed, H. Sayour, F. Canfarotta, S. Piletsky, M.A.M. Soliman, Functionalized core-shell yttrium oxide nanoparticles as antioxidants agents in heat stressed rats, Biol. Trace Elem. Res. 198 (2020) 189–197.
[38] Z. Zhang, H. Suo, X. Zhao, D. Sun, L. Fan, C. Guo, NIR-to-NIR deep penetrating nanoplatforms Y_2O_3:Nd^{3+}/Yb^{3+}@SiO_2@Cu_2S toward highly efficient photothermal ablation, ACS Appl. Mater. Interfaces 10 (2018) 14570–14576.
[39] C.A. Traina, T.J. Dennes, J. Schwartz, A modular monolayer coating enables cell targeting by luminescent yttria nanoparticles, Bioconj. Chem. 20 (2009) 437–439.
[40] K. Soga, K. Tokuzen, K. Tsuji, T. Yamano, H. Hyodo, H. Kishimoto, NIR bioimaging: development of liposome-encapsulated, rare-earth-doped Y_2O_3 nanoparticles as fluorescent probes, Eur. J. Inorg. Chem. 2010 (2010) 2673–2677.
[41] G.K. Das, T.T.Y. Tan, Rare-earth-doped and codoped Y_2O_3 nanomaterials as potential bioimaging probes, J. Phys. Chem. C. 112 (2008) 11211–11217.

[42] M. Chang, S. Tie, Fabrication of novel luminor $Y_2O_3:Eu^{3+}$@SiO_2@$YVO_4:Eu^{3+}$ with core/shell heteronanostructure, Nanotechnology 19 (2008) 075711.

[43] A. Nexha, M.C. Pujol, F. Díaz, M. Aguiló, J.J. Carvajal, Luminescence nanothermometry using self-assembled Er^{3+}, Yb^{3+} doped Y_2O_3 nanodiscs: might the upconversion mechanism condition their use as primary thermometers? Opt. Mater. 134 (2022) 113216.

[44] A. Nexha, J.J. Carvajal, M.C. Pujol, F. Díaz, M. Aguiló, Lanthanide doped luminescence nanothermometers in the biological windows: strategies and applications, Nanoscale 13 (2021) 7913–7987.

[45] F. Vetrone, J.C. Boyer, J.A. Capobianco, A. Speghini, M. Bettinelli, Effect of Yb^{3+} codoping on the upconversion emission in nanocrystalline $Y_2O_3:Er^{3+}$, J. Phys. Chem. B 107 (2003) 1107–1112.

[46] A.O.G. Dikovska, P.A. Atanasov, M. Jiménez de Castro, A. Perea, J. Gonzalo, C. N. Afonso, J. García López, Optically active Er^{3+}-Yb^{3+} codoped Y_2O_3 films produced by pulsed laser deposition, Thin Solid Films 500 (2006) 336–340.

[47] S.F. Lim, R. Riehn, W.S. Ryu, N. Khanarian, C. Tung, D. Tank, R.H. Austin, In Vivo and scanning electron microscopy imaging of upconverting nanophosphors in caenorhabditis elegans, Nano Lett. 6 (2006) 169–174.

[48] H. Huang, X. Sun, S. Wang, Y. Liu, X. Li, J. Liu, Z. Kang, S.T. Lee, Strong red emission of pure Y_2O_3 nanoparticles from oxygen related defects, Dalton Trans. 40 (2011) 11362–11366.

[49] M. Jublot, F. Paumier, F. Pailloux, B. Lacroix, E. Leau, P. Guérin, M. Marteau, M. Jaouen, R.J. Gaboriaud, D. Imhoff, Yttrium oxide thin films: influence of the oxygen vacancy network organization on the microstructure, Thin Solid Films 515 (2007) 6385–6390.

[50] C.G. Enke, Nonstoichiometry, diffusion, and electrical conductivity in binary metal oxides, Mater. Corros. 25 (1974) 801–802.

[51] L. Alvarez, M. San-Miguel, J. Odriozola, Effects of nonstoichiometry in the melting process of Y_2O_3 from molecular dynamics simulations, Phys. Rev. B 591 (1999), 1126458-1111307.

[52] B.T. Kilbourn, Yttria, in: R.J. Brook (Ed.) Concise Encyclopedia of Advanced Ceramic Materials, Pergamon, Oxford, 1991, pp. 521–522.

[53] R. Mellado-Vázquez, M. García-Hernández, A. López-Marure, P.Y. López-Camacho, Á. de Jesús Morales-Ramírez, H.I. Beltrán-Conde, Sol-gel synthesis and antioxidant properties of yttrium oxide nanocrystallites incorporating P-123, Materials 7 (2014) 6768–6778.

[54] D. Wang, Y. Kang, X. Ye, C.B. Murray, Mineralizer-assisted shape-control of rare earth oxide nanoplates, Chem. Mater. 26 (2014) 6328–6332.

[55] J. Jeong, N. Kim, M.G. Kim, W. Kim, Generic synthetic route to monodisperse sub-10 nm lanthanide oxide nanodisks: a modified digestive ripening process, Chem. Mater. 28 (2016) 172–179.

[56] Z. Li, T. Liang, S. Lv, Q. Zhuang, Z. Liu, A rationally designed upconversion nanoprobe for in vivo detection of hydroxyl radical, J. Am. Chem. Soc. 137 (2015) 11179–11185.

[57] Y. Zhai, K. Zhou, Y. Xue, F. Qin, L. Yang, X. Yao, Synthesis of water-soluble chitosan-coated nanoceria with excellent antioxidant properties, RSC Adv. 3 (2013) 6833–6838.

[58] D. Heck, M. Shakarjian, H. Kim, D. Laskin, A. Vetrano, Mechanisms of oxidant generation by catalase, Ann. N. Y. Acad. Sci. 1203 (2010) 120–125.

[59] D. Engelsen, G. Fern, T. Ireland, D. Hudry, M. Abeykoon, D. Nykypanchuk, J. Dickerson, J. Silver, Ultrathin $Y_2O_3:Eu^{3+}$ nanodiscs: spectroscopic investigations and evidence for reduced concentration quenching, Nanotechnology 29 (2018).

[60] D. den Engelsen, B. de Koning, Ellipsometric study of organic monolayers. Part 1. Condensed monolayers, J. Chem. Soc. Faraday Trans. 70 (1974) 1603–1614.

[61] M. Klokkenburg, J. Hilhorst, B.H. Erné, Surface analysis of magnetite nanoparticles in cyclohexane solutions of oleic acid and oleylamine, Vib. Spectrosc. 43 (2007) 243–248.

[62] R. Si, Y.W. Zhang, H.P. Zhou, L.D. Sun, C.H. Yan, Controlled-synthesis, self-assembly behavior, and surface-dependent optical properties of high-quality rare-earth oxide nanocrystals, Chem. Mater. 19 (2007) 18–27.

[63] J. He, P. Kanjanaboos, N.L. Frazer, A. Weis, X.M. Lin, H.M. Jaeger, Fabrication and mechanical properties of large-scale freestanding nanoparticle membranes, Small 6 (2010) 1449–1456.

[64] L. Zhang, R. He, H.C. Gu, Oleic acid coating on the monodisperse magnetite nanoparticles, Appl. Surf. Sci. 253 (2006) 2611–2617.

[65] E.D. Smolensky, H.Y.E. Park, T.S. Berquó, V.C. Pierre, Surface functionalization of magnetic iron oxide nanoparticles for MRI applications-effect of anchoring group and ligand exchange protocol, Contrast Media Mol. Imaging 6 (2011) 189–199.

[66] K. Ahrenstorf, H. Heller, A. Kornowski, J.A.C. Broekaert, H. Weller, Nucleation and growth mechanism of Ni_xPt_{1-x} nanoparticles, Adv. Funct. Mater. 18 (2008) 3850–3856.

[67] A. Nelson, Y. Zong, K.E. Fritz, J. Suntivich, R.D. Robinson, Assessment of soft ligand removal strategies: akylation as a promising alternative to high-temperature treatments for colloidal nanoparticle surfaces, ACS Mater. Lett. 1 (2019) 177–184.

[68] A. Dong, X. Ye, J. Chen, Y. Kang, T. Gordon, J.M. Kikkawa, C.B. Murray, A generalized ligand-exchange strategy enabling sequential surface functionalization of colloidal nanocrystals, J. Am. Chem. Soc. 133 (2011) 998–1006.

[69] F.M. Nicolaisen, IR absorption spectrum (4200-3100cm^{-1}) of H_2O and $(H_2O)_2$ in CCl_4. estimates of the equilibrium constant and evidence that the atmospheric water absorption continuum is due to the water dimer, J. Quant. Spectrosc. Radiat. Transf. 110 (2009) 2060–2076.

[70] P. Attri, Y.H. Kim, D.H. Park, J.H. Park, Y.J. Hong, H.S. Uhm, K.-N. Kim, A. Fridman, E.H. Choi, Generation mechanism of hydroxyl radical species and its lifetime prediction during the plasma-initiated ultraviolet (UV) photolysis, Sci. Rep. 5 (2015) 9332.

[71] X. Yang, P. Tian, X. Zhang, X. Yu, T. Wu, J. Xu, Y. Han, The generation of hydroxyl radicals by hydrogen peroxide decomposition on FeOCl/SBA-15 catalysts for phenol degradation, AIChE J. 61 (2015) 166–176.

[72] J. Korppi-Tommola, R. Yip, Solvent effects on the visible absorption spectrum of crystal violet, Can. J. Chem. 59 (2011) 191–194.

[73] S.Y. Yao, W.Q. Xu, A.C. Johnston-Peck, F.Z. Zhao, Z.Y. Liu, S. Luo, S. D. Senanayake, A. Martínez-Arias, W.J. Liu, J.A. Rodriguez, Morphological effects of the nanostructured ceria support on the activity and stability of CuO/CeO_2 catalysts for the water-gas shift reaction, Phys. Chem. Chem. Phys. 16 (2014) 17183–17195.

[74] M. Lu, Y. Zhang, Y. Wang, M. Jiang, X. Yao, Insight into several factors that affect the conversion between antioxidant and oxidant activities of nanoceria, ACS Appl. Mater. Interfaces 8 (2016) 23580–23590.

[75] B. Chance, The composition of catalase-peroxide complexes, J. Biol. Chem. 179 (1949) 1311–1330.

[76] A. Deisseroth, A.L. Dounce, Catalase: physical and chemical properties, mechanism of catalysis, and physiological role, Physiol. Rev. 50 (1970) 319–375.

[77] K. Cikalleshi, A. Nexha, T. Kister, M. Ronzan, A. Mondini, S. Mariani, T. Kraus, B. Mazzolai, A printed luminescent flier inspired by plant seeds for eco-friendly physical sensing, Sci. Adv. 9 (2023) eadi8492.

[78] A. Nexha, M.C. Pujol Baiges, J.J. Carvajal Martí, Luminescent nanothermometers operating within biological windows, in: {C}J.J. Carvajal Martí, M.C. Pujol Baiges {C} (Eds.) Luminescent Thermometry: Applications and Uses, Springer International Publishing, Cham, 2023, pp. 221–268.